Inorganic Chemistry

Article

pubs.acs.org/IC

Increase in the Coordination Number of a Cobalt Porphyrin after Photo-Induced Interfacial Electron Transfer into Nanocrystalline TiO_2

Darren Achey,[†] Shane Ardo,[†] and Gerald J. Meyer*[,†,‡]

[†]Department of Chemistry and [‡]Department of Materials Science & Engineering, Johns Hopkins University, 3400 North Charles Street, Baltimore, Maryland 21218, United States

Supporting Information

ABSTRACT: Spectroscopic, electrochemical, and kinetic data provide compelling evidence for a coordination number increase initiated by interfacial electron transfer. Light excitation of Co^{I}(*meso*-5,10,15,20-tetrakis(4-carboxyphenyl)porphyrin) anchored to a nanocrystalline TiO_2 thin film, abbreviated $Co^{I}P/TiO_2$, immersed in an acetonitrile:pyridine electrolyte resulted in rapid excited state injection, $k_{inj} > 10^8\ s^{-1}$, to yield $Co^{II}P/TiO_2(e^-)$, followed by axial coordination of pyridine to the $Co^{II}P$ and hence an increase in coordination number from four to five. The formal oxidation state and coordination environment of the Co metalloporphyrin on TiO_2 were assigned through comparative studies in fluid solution as well as by comparisons to previously reported data. The kinetics for pyridine coordination were successfully modeled with a pseudo-first order kinetic model that yielded a second-order rate constant of $k_{+py} = 2 \times 10^8\ M^{-1}\ s^{-1}$. Spectro-electrochemical measurements showed that pyridine coordination resulted in a ~200 mV negative shift in the $Co^{II/I}$ reduction potential, $E°(Co^{II/I}/TiO_2) = -0.72$ V and $E°(Co^{II/I}(py)/TiO_2) = -0.85$ V vs NHE. With some assumptions, this indicated an equilibrium formation constant $K_f = 400\ M^{-1}$ for the $Co^{II}P(py)/TiO_2$ compound. The kinetics for charge recombination were non-exponential under all conditions studied, but were successfully modeled by the Kohlrausch–Williams–Watts (KWW) function with observed rate constants that decreased by about a factor of 100 when pyridine was present. The possible mechanisms for charge recombination are discussed.

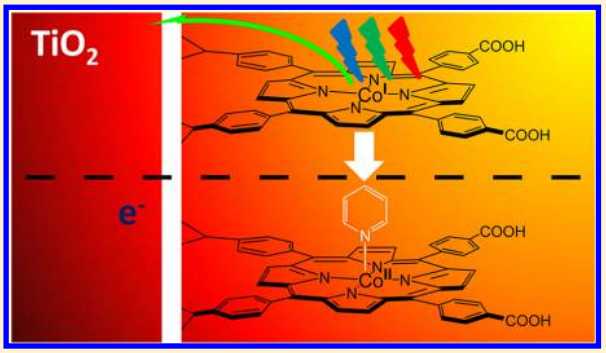

INTRODUCTION

Electron transfer from a molecular excited state to a semiconductor material provides a means for conversion of the free energy stored in the excited state into a charge separated state composed of an oxidized molecule and a reduced semiconductor.[1,2] An advantage of separating charges at conductive interfaces is that one of the redox equivalents formed can transport from the interface to an external location where subsequent redox reactions are initiated. For example, in regenerative dye-sensitized solar cells, an electron injected into TiO_2 transports to a Pt electrode where tri-iodide is reduced.[3] In what have been termed photoelectrosynthetic cells for water oxidation, injected electrons reduce protons and generate hydrogen gas at an external electrode.[4,5]

In older embodiments of photoelectrosynthetic cells, the oxidized dye molecule itself was proposed to drive the multielectron transfer reactions necessary for water oxidation.[6,7] The mechanistic details that have recently emerged for molecular water oxidation, and other multielectron transfer reactions relevant to solar fuel generation, consistently invoke inner-sphere activation with transition metal catalysts.[8−10] Therefore, if one attempts to use a single coordination compound to sensitize a wide bandgap semiconductor to visible light *and* drive catalysis, open coordination sites may be necessary. Unfortunately, the most stable and widely utilized Ru polypyridyl sensitizers are substitution-inert coordinatively saturated octahedral compounds.[2]

We recently reported excited-state electron injection into mesoporous, nanocrystalline TiO_2 films by cobalt *meso*-5,10,15,20-tetrakis(4-carboxyphenyl) porphyrin (CoP) when in the formal oxidation state of Co^{I}.[11] Well documented in the Vitamin B12 (cobalamin) and cobalt porphyrin literature is the tendency of Co to ligate a specific number of axial ligands in a given oxidation state: Co^{III} has two axial ligands, Co^{II} has one axial ligand, and Co^{I} has no axial ligands.[12,13] An example of this for pyridine ligation to a cobalt macrocycle is shown in Scheme 1. With this background, it seemed likely that after $Co^{I}P^*/TiO_2 \rightarrow Co^{II}P/TiO_2(e^-)$ excited-state injection, the $Co^{II}P$ generated

Scheme 1. Typical Axial Ligation of Pyridine to a Co Macrocycle in the Indicated Formal Oxidation States

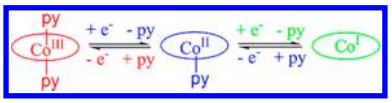

Received: June 19, 2012

   dx.doi.org/10.1021/ic301300h | *Inorg. Chem.* XXXX, XXX, XXX–XXX

would ligate a fifth ligand. Here we present compelling evidence that this does indeed occur. While light-induced coordination number changes have been observed for excited and charge-separated states in fluid solution, to our knowledge this report represents the first example initiated by photoinduced interfacial electron transfer.[14−17] Whether this finding can one day be exploited for photocatalysis remains to be demonstrated. More fundamentally, inner-sphere ligation provides a general means by which the thermodynamics and kinetics for the unwanted $Co^{II}P/TiO_2(e^-) \rightarrow Co^{I}P/TiO_2$ charge recombination reaction can be controlled. In one extreme, ligand dissociation and charge recombination occur in one concerted step such that the enthalpic contribution of breaking the Co-ligand bond is included within the total reorganization energy for electron transfer. Indeed, it is shown herein that charge recombination is significantly slowed by inner-sphere coordination of pyridine.

EXPERIMENTAL SECTION

Materials. The following reagents were used as received from the indicated commercial suppliers: acetonitrile (Burdick and Jackson, spectrophotometric grade); dimethylsulfoxide (DMSO; Fisher Scientific, 99.9%); pyridine (py; Fisher Scientific, 99.9%); deionized water; acetone (bulk solvent); tetra-*n*-butylammonium perchlorate (TBA-ClO_4; Fluka, >99.9%); tetra-n-butylammonium hydroxide (TBAOH; Fluka 1 M aqueous); cobalt(III) *meso*-5,10,15,20-tetrakis(4-carboxyphenyl)porphyrin chloride (CoP; Frontier Scientific >97%); argon gas (Airgas, >99.998%); oxygen gas (Airgas, industrial grade); titanium(IV)isopropoxide (Sigma-Aldrich, 97%); fluorine-doped SnO_2-coated glass (FTO; Hartford Glass Co., Inc., 2.3 mm thick, 15 Ω/□); glass microscope slides (Fisher Scientific, 1 mm thick); and triethylamine (Fisher Scientific, 99%).

[*fac*-Re(deeb)$(CO)_3$(4-ethylpyridine)](OTf), where OTf^- is triflate anion and deeb is 4,4′ diethylester-2,2′ bipyridine, was prepared as previously described.[18,19]

Preparations. *Sensitized Metal-Oxide Thin Film Electrode.* Transparent TiO_2 nanocrystallites (anatase, ∼15 nm diameter) were prepared by hydrolysis of Ti(*i*-OPr)$_4$ using a sol−gel technique previously described in the literature.[20] The sols were cast as mesoporous thin films (∼ 5 μm thick), using Scotch tape as a spacer, by doctor blading onto transparent FTO conductive substrates. The thin films were annealed at 420 °C for 30 min under an atmosphere of O_2 flow.

The films were pretreated with aqueous base (TBAOH, pH ∼ 11) for 10 min, followed by an acetonitrile wash, and were then immersed in a μM CoP/DMSO solution. Within an hour, the films became brightly colored and were washed thoroughly with 100 mM $TBAClO_4$/acetonitrile and placed diagonally in a standard 1 cm^2 quartz cuvette containing the electrolyte solution. The electrolyte solution were purged with Ar(g) for at least 30 min prior to experimentation. The surface coverage, Γ, in mol/cm^2, was quantified from the measured absorption data with the modified Beer−Lambert formula given in eq 1,

$$\text{Abs} = 1000 \times \Gamma \times \varepsilon \quad (1)$$

where ε is the molar decadic extinction (absorption) coefficient, M^{-1} cm^{-1}, that was assumed to be unchanged whether in solution or on the surface. The cobalt porphyrins were typically anchored to the films in coverages of $\Gamma = 1-4 \times 10^{-9}$ mol/cm^2. These values are equivalent to approximately 10% of the saturation surface coverage.

Spectroscopy. Steady-state UV−visible absorption spectra were obtained on either a Varian Cary 50 spectrophotometer or a Hewlett-Packard 8453 Photodiode Array UV−vis Spectrophotometer at room temperature. Nanosecond transient absorption were obtained on an apparatus similar to that which has been previously described.[21] Samples were irradiated with 532 nm light from a frequency doubled Q-switched, pulsed Nd:YAG laser (Quantel U.S.A. (BigSky) Brilliant B; 5−6 ns full width at half-maximum, 1 Hz, ∼ 10 mm in diameter) directed 45° to the FTO side of a TiO_2 film. The excitation fluence was measured by a thermopile power meter (Molectron) and was typically <2 mJ/cm^2. A 150 W xenon arc lamp served as the probe beam (Applied Photophysics) that was aligned orthogonally to the laser excitation and directed to a monochromator (Spex 1702/04) optically coupled to an R928 photomultiplier tube (Hamamatsu). Transient data were acquired on a computer-interfaced 350 MHz digital oscilloscope (LeCroy 9450). In typical experiments, 30 laser pulses were averaged at each monitoring wavelength, and full spectra were generated by averaging multiple data points.

Electrochemistry. Electrochemical measurements utilized a potentiostat (BAS model CV-50W or Epsilon electrochemical analyzer) with a standard three electrode arrangement with a glassy carbon disk (solution) or sensitized TiO_2 thin film deposited on FTO glass (surface) working electrode, a Pt gauze or Pt disk (Bioanalytical Scientific Instruments, Inc.) counter electrode, and an aqueous Ag/AgCl (KCl saturated) reference electrode. All potentials are reported vs NHE unless otherwise noted. The ferrocenium/ferrocene ($Fe(Cp)_2^{+/0}$) half-wave potential was measured both before and after experiment in a 100 mM $TBAClO_4$/acetonitrile electrolyte and was used as a standard to calibrate the reference electrode. Conversion to vs NHE was achieved by correcting for the expected ferrocenium/ferrocene $E_{1/2}$ of +310 mV vs the KCl-saturated aqueous calomel electrode (SCE), where SCE is +241 mV vs NHE.[22]

The reduction potentials for CoP in fluid solution were determined by differential pulse voltammetry as an average of the anodic and cathodic peak potentials.

Spectroelectrochemistry was executed through simultaneous application of an applied potential bias while monitoring the UV−vis absorption spectra of TiO_2 thin film electrodes in the standard electrolytes. At each potential step, a spectrum that was invariant with time was recorded. Single-wavelength absorption features plotted as a function of potential bias were proportional to the cumulative formation/loss of states; for the $TiO_2(e^-)$ absorption features this was directly related to the cumulative TiO_2 density of states.

Reductive Photochemistry. Photochemical reduction of ∼5 μM CoP was performed in argon-purged acetonitrile/DMSO (∼ 1% v/v of DMSO) or acetonitrile/pyridine (∼ 15% v/v of pyridine) solutions containing ∼50 μM [*fac*-Re(deeb)$(CO)_3$(4-ethylpyridine)](OTf) and 50 mM triethylamine. A lens focused 150 W Xe arc lamp was utilized as the photolysis source and absorption spectra were recorded perpendicular to the light excitation.

RESULTS

Steady-state illumination of [Re$(CO)_3$(deeb)(4-ethyl pyridine)](OTf), where OTf^- is triflate anion and deeb is 4,4′-diethylester-2,2′-bipyridine, in the presence of a sacrificial electron donor, triethylamine (TEA), and $Co^{III}P$, where P is *meso*-5,10,15,20-tetrakis(4-carboxyphenyl)porphyrin, in an acetonitrile:DMSO solution, 1:100 (v/v), resulted in spectral changes associated with reduction of the Co^{III} metal center to Co^{II}, followed by further reduction to Co^{I}, and finally observation of the reduced Re complex, [Re$(CO)_3$(deeb$^-$)(4-ethyl pyridine)]. These photochemical experiments were repeated in the added presence of ∼2 M pyridine where the same sequence of redox reactions was observed. Representative extinction coefficient spectra for the metalloporphyrin in the indicated oxidation states in the absence, CoP, and presence of 2 M pyridine, CoP(py), are shown in Figure 1. Note that the CoP(py) abbreviation refers only to the presence of pyridine and does not imply a specific number of coordinated pyridines. The minor visible absorption from [Re$(CO)_3$(deeb)(4-ethyl pyridine)]-(OTf) or [Re$(CO)_3$(deeb$^-$)(4-ethyl pyridine)] were subtracted from the spectral data shown in Figure 1.

The $Co^{III}P$ compound was anchored to a mesoporous, nanocrystalline TiO_2 (anatase) thin film supported on a fluorine doped tin oxide (FTO) glass electrode, herein abbreviated CoP/TiO_2, and immersed in an argon-saturated 100 mM $TBAClO_4$ acetonitrile solution. Typical surface coverages were $1-4 \times 10^{-9}$

dx.doi.org/10.1021/ic301300h | Inorg. Chem. XXXX, XXX, XXX−XXX

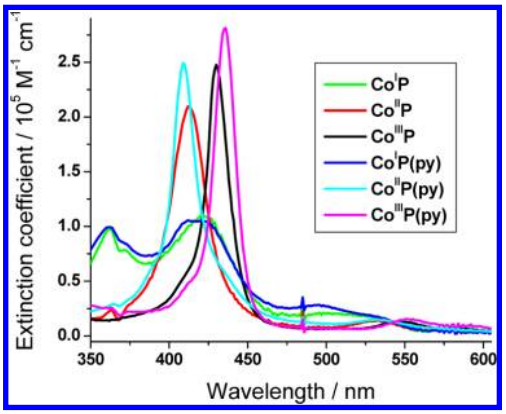

Figure 1. Extinction coefficient spectra of CoP in the indicated formal oxidation states in the absence and presence of 2 M pyridine (py) measured in argon-purged acetonitrile:DMSO 1:100 (v/v) solution with 50 mM triethylamine.

mol/cm^2. The visible absorption spectra of $Co^{III}P/TiO_2$ immersed in DMSO were, within experimental error, the same as that for the compound dissolved in fluid solution. The CoP/TiO_2 thin film was used as the working electrode in a standard 3-electrode electrochemical cell positioned in a 1 cm cuvette in a UV−vis spectrophotometer. Forward bias raised the Fermi level of the functionalized film, with spectral changes associated with the reduction of the Co^{III} center to the formal oxidation state of Co^{II}, followed by the appearance of absorption features characteristic of reduced TiO_2, abbreviated as $TiO_2(e^-)$ and shown in Supporting Information, Figure S1. As the Fermi level was raised further an increase in the $TiO_2(e^-)$ concentration was observed concurrent with the reduction of $Co^{II}/TiO_2(e^-)$ to $Co^{I}/TiO_2(e^-)$. The same sequence of redox processes were observed when 360 mM pyridine was present in the electrolyte solution, herein abbreviated as CoP(py)/TiO_2. Representative absorption spectra of CoP/TiO_2 and CoP(py)/TiO_2 after spectral features from the $TiO_2(e^-)$s were subtracted in the indicated oxidation states are shown in Figure 2A. Figure 2B shows absorption difference spectra measured after complete conversion of $Co^{I}P/TiO_2$ to $Co^{II}P/TiO_2$ in the presence (red) and absence (black) of pyridine. Of note in Figure 2B were the unique Co^{II}−Co^{I} isosbestic points observed with (426 nm) and without (432 nm) pyridine as well as the sharper, more intense absorption band at 410 nm observed when pyridine was present.

Figure 3 presents the absorbance monitored at 373 and 800 nm as a function of applied potential for a CoP/TiO_2 thin film in

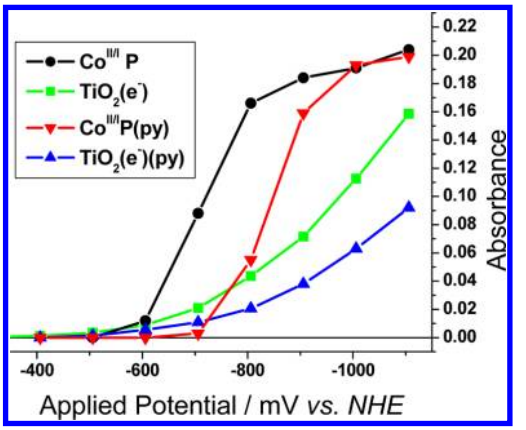

Figure 3. Absorbance measured at 373 and 800 nm as a function of applied potential for a CoP/TiO_2 thin-film electrode immersed in 0.1 M $TBAClO_4$ in acetonitrile in the absence and presence of 360 mM pyridine. The 373 nm data reported on the formation of $Co^{I}P/TiO_2$ while the absorbance at 800 nm was due to $TiO_2(e^-)$s.

0.1 M $TBAClO_4$/acetonitrile, both with (red and blue) and without (black and green) 360 mM pyridine. An isosbestic point for the appearance of $TiO_2(e^-)$ was measured at 373 nm; therefore, measurements at this wavelength reported only on the reduction of $Co^{II}P/TiO_2$ to $Co^{I}P/TiO_2$. The 800 nm absorption was due solely to $TiO_2(e^-)$s.

The 800 nm absorption data were fit to an exponential function while the 373 nm data were fit with eq 2,[23]

$$x = \frac{1}{1 + 10^{(E_{app} - E^0)/(a \times 59\ \mathrm{mV})}} \quad (2)$$

where x is the fraction of the CoP in the Co^{I} oxidation state, E_{app} is the applied potential, E^0 is the formal reduction potential, and a is the ideality factor that accounts for the non-Nernstian behavior of the reduction. The ideality factor was 2.2 when the measurements were made in the absence of pyridine, compared to 1.6 in the presence of pyridine.

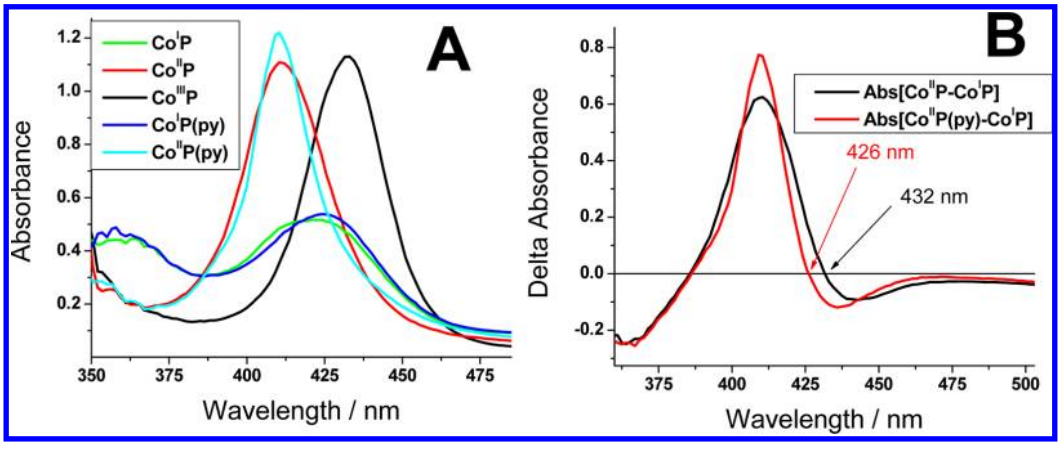

Figure 2. (A) Absorption spectra of a CoP/TiO_2 thin-film in the indicated formal oxidation states measured in 100 mM $TBAClO_4/CH_3CN$ electrolyte with and without 360 mM pyridine (py). (B) The $Co^{II}P/TiO_2$ absorption spectrum minus the $Co^{I}P/TiO_2$ absorption spectrum with noted isosbestic points measured with (red) and without (black) 360 mM pyridine.

dx.doi.org/10.1021/ic301300h | Inorg. Chem. XXXX, XXX, XXX−XXX

The derivatives of the $Co^{II/I}$ concentrations extracted from the spectroelectrochemical data as well as the exponential distribution of the $TiO_2(e^-)$s both versus applied potential were plotted as the chemical capacitance as shown in Figure 4.

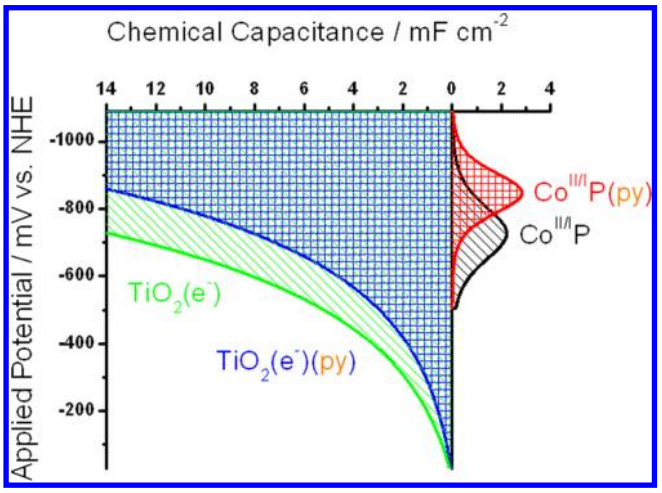

Figure 4. Chemical capacitance of a CoP/TiO_2 thin-film electrode immersed in 0.1 M $TBAClO_4/CH_3CN$ in the absence and presence of 360 mM pyridine as a function of applied potential.

The CoP formal reduction potentials, ideality factors, and absorbance data in the presence and absence of pyridine, both anchored to TiO_2 and in solution are summarized in Table 1. The

Table 1. $Co^{II/I}P$ Reduction Potentials and Ideality Factors, *a*

sample	$E°(Co^{II/I})$ V vs NHE	*a*
CoP/TiO_2	−0.72	2.2 ± 0.1
$CoP(py)/TiO_2$[i]	−0.85	1.6 ± 0.1
CoP/DMSO	−0.61	
CoP(py)[ii]	−0.83	

[i]Measured in acetonitrile with 0.36 M pyridine. [ii]Measured in neat pyridine, 12.4 M.

solution $E_{1/2}$ values were obtained via differential pulse voltammetry in 0.1 M $TBAClO_4$ solutions of both DMSO (CoP is insoluble in acetonitrile) and pyridine. The $Co^{II/I}P/TiO_2$ reduction potentials in acetonitrile and acetonitrile/pyridine solutions were taken to be the equilibrium potential at which 50% of the surface-bound molecules were reduced to the Co^{I} state in the spectroelectrochemical experiment shown in Figure 3.

The equilibrium constant for axial ligation of pyridine to $Co^{II}P$ measured relative to DMSO was determined by electrochemical measurements as previously described.[13] The use of DMSO was required because of poor solubility of $Co^{III}P$ in CH_3CN. The half-wave potentials in DMSO and pyridine electrolyte, $E_{1/2}Co^{II/I}_{(py)}$ and $E_{1/2}Co^{II/I}_{(DMSO)}$, were measured by differential pulse voltammetry. These potentials were used in conjunction with eq 3

$$E_{1/2}Co^{II/I}_{(py)} = E_{1/2}Co^{II/I}_{(DMSO)} - 0.059 \times \log(K_{Co^{II}\text{-}py}) - 0.059 \times \log[py] \quad (3)$$

to calculate the equilibrium constant for pyridine ligation to $Co^{II}P$, $K_{Co^{II}\text{-}py}$. A value of ~400 M^{-1} ($\log(K_{Co^{II}\text{-}py}) = 2.6 \pm 0.3$) was calculated. The equilibrium constant for pyridine ligation to $Co^{II}P/TiO_2$ with respect to CH_3CN was calculated based on the spectroelectrochemical data in Table 1 and yielded $\log(K_{Co^{II}\text{-}py})$ of 2.6 ± 0.3.

Shown in Figure 5 are transient absorption spectra measured at the indicated delay times after pulsed 532 nm laser excitation of a $Co^{I}P/TiO_2$ thin film immersed in 0.1 M $TBAClO_4/CH_3CN$ with 0, 0.03, and 2.5 M pyridine. When no pyridine was present in the external solution, the spectra recorded at each delay time were within experimental error the same when normalized. The contribution due to $TiO_2(e^-)$s over this wavelength range was very small and thus afforded realistic $Co^{II/I}P/TiO_2$ isosbestic points. At the extreme of ~2.5 M pyridine in Figure 5C, the measured spectra were again unchanged when normalized, but with an isosbestic point at 426 nm. At intermediate pyridine concentrations (0.03 M), Figure 5B, an isosbestic point at 432 nm was initially observed that shifted to 426 nm at observation times longer than 3 μs. Under these conditions, the spectra observed at delay times less than 3 μs were time dependent.

The transient absorption decay monitored at 415 nm, the approximate $Co^{II}P/Co^{II}P(py)$ isosbestic point, was measured at different pyridine concentrations with a constant applied bias of −920 mV vs NHE, Figure 6A. At this observation wavelength, spectral features due to charge recombination between the injected electron and the oxidized cobalt compound, that is, $TiO_2(e^-) + Co^{II}P \rightarrow TiO_2 + Co^{I}P$, were observed without contribution from pyridine ligation. The data were satisfactorily fit to the Kohlrausch–Williams–Watts (KWW) function, eq 4,[24,25]

$$I(t) = I_0 \exp[-(k_{obs}t)^{\beta}] \quad (4)$$

where β is inversely related to the width of a Lèvy distribution of rate constants, and was fixed at 0.365. Increased pyridine concentrations resulted in slower loss of the absorption change associated with Co^{II}. Shown in Figure 6B are absorption decays monitored at 426 nm where two competitive processes were expected: charge recombination and pyridine association to Co^{II}. The kinetic data was therefore fit to a kinetic model based on a sum of a KWW function (with k_{obs} and β fixed from the 415 nm data) and a first-order reaction. Therefore, data monitored at 426 nm on these time scales reported on the coordination of pyridine to Co^{II} and was adequately described by a pseudo-first order kinetic model at high pyridine concentrations. Plots of the abstracted rate pseudo-first order rate constants measured as a function of pyridine concentration from 4–20 mM were linear and yield a second order rate constant of $2 \pm 1 \times 10^8$ M^{-1} s^{-1}, Figure 6B inset.

Shown in Figure 7 are plots of the observed rate constants versus the 800 nm absorbance at the indicated pyridine concentrations. The observed rate constants, k_{obs}, were measured as a function of applied bias, which was used to control the concentration of $TiO_2(e^-)$ as was quantified through their absorption at 800 nm. The 800 nm absorbance was measured directly for the extreme pyridine concentrations of 0 and 0.36 M, intermediate values were approximated based on a logarithmic dependence of the $[TiO_2(e^-)]$ with pyridine concentration. The absorbance at 800 nm was converted to the number of $TiO_2(e^-)$s in a 1 cm^2 geometric area by eq 1, using a molar decadic extinction coefficient of 1000 M^{-1} cm^{-1}.[2]

DISCUSSION

The results presented herein illustrate the first instance of an excited state interfacial electron transfer event that initiates

dx.doi.org/10.1021/ic301300h | Inorg. Chem. XXXX, XXX, XXX–XXX

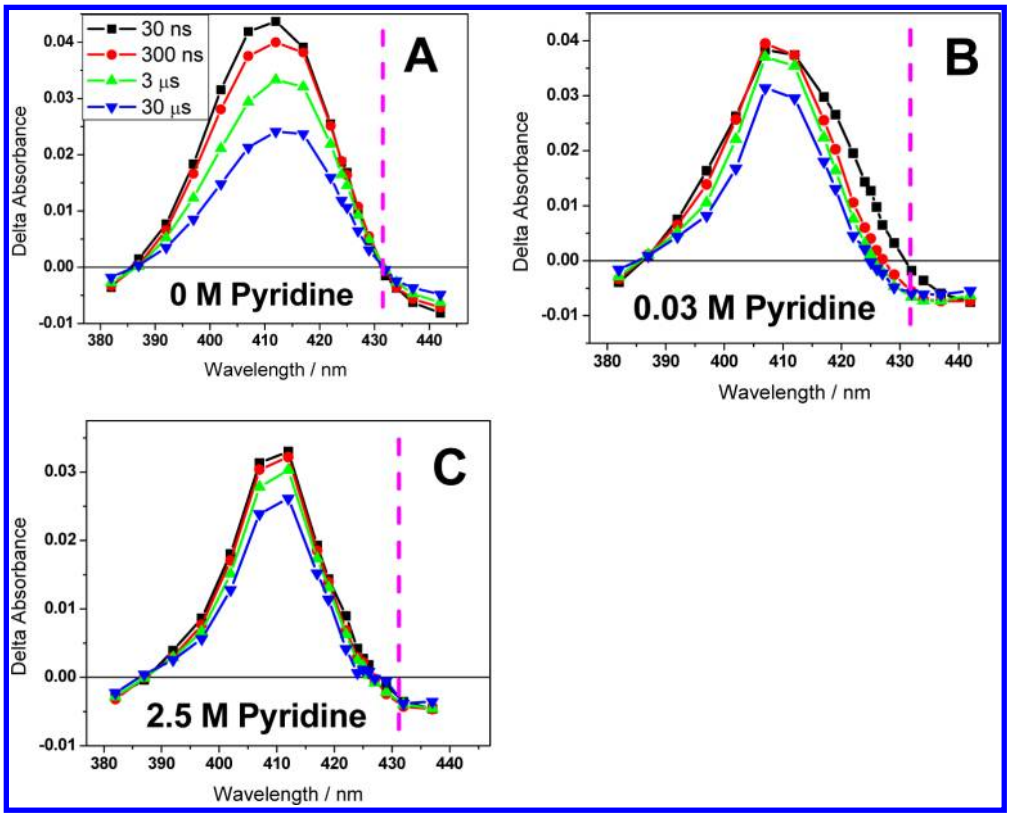

Figure 5. Transient absorption data collected at the indicated delay times following pulsed 532 nm laser excitation of a $Co^{I}P/TiO_2$ thin film immersed in 0.1 M $TBAClO_4/CH_3CN$ with the indicated pyridine concentrations. For reference, the vertical dashed line indicates the 432 nm isosbestic point for Co^{II} to Co^{I} reduction in the absence of pyridine.

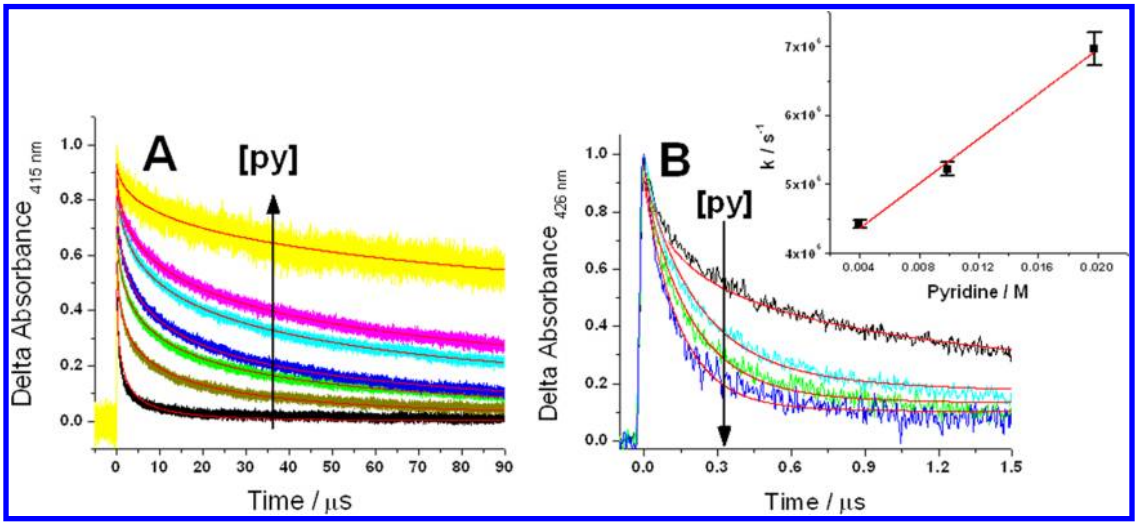

Figure 6. (**A**) Absorption change monitored at 415 nm (indicative of charge recombination) under the same experimental conditions from Figure 5 with 0 to 0.3 M pyridine. A bias of −920 mV vs NHE was applied throughout the experiment, and the data were normalized to the maximum signal. Overlaid on the data are kinetic fits to the KWW model. (**B**) Absorption change monitored at 426 nm (indicative of pyridine ligation) for a CoP/TiO_2 thin film with increasing pyridine concentrations at an applied bias of −830 mV vs NHE. Overlaid on the black data (0 M pyridine) in red is a fit to the KWW model, the other three data have overlaid fits to a sum of a KWW and a first-order kinetic model. In both **A** and **B** the direction of the arrow indicates increasing pyridine concentrations. The inset illustrates the observed first-order rate constants as a function of titrated pyridine concentration.

formation of a metal−ligand bond and hence an increase in the coordination number. Light excitation of $Co^{I}P/TiO_2$ resulted in rapid interfacial electron transfer to yield $Co^{II}P/TiO_2(e^-)$, followed by ligation of pyridine to the Co^{II} metal center. Pyridine ligation was found to alter the thermodynamics and kinetics for electron transfer as is described further below.

Interfacial Thermodynamics. Spectroelectrochemistry was utilized as an in situ tool to characterize the interfacial redox thermodynamics of CoP/TiO_2 with and without pyridine in the external acetonitrile electrolyte that surrounded the sensitized thin film. The cobalt sensitizer was anchored to TiO_2 in the formal oxidation state of Co^{III}. By raising the Fermi-level of the sensitized TiO_2 film toward the vacuum level with an external

dx.doi.org/10.1021/ic301300h | Inorg. Chem. XXXX, XXX, XXX−XXX

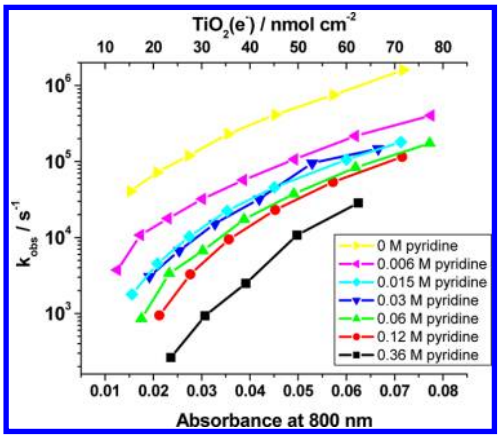

Figure 7. Observed rate constants for charge recombination measured at 415 nm after pulsed 532 nm laser excitation of a potentiostatically controlled $Co^{I}P/TiO_2$ thin film in acetonitrile electrolyte with the indicated pyridine concentration. The rate constant data are plotted versus the absorbance at 800 nm, which is directly related to the $TiO_2(e^-)$ concentration.

bias, the reduction of Co^{III} to Co^{II} was first observed followed by the reduction of TiO_2 itself, abbreviated $TiO_2(e^-)$, and finally the reduction of Co^{II} to Co^{I}. In all cases, the spectral changes that accompanied this redox chemistry were reversible with maintenance of isosbestic points when the applied bias was reversed. The formal oxidation states of CoP were unambiguously assigned by independent characterization of the metalloporphyrin in fluid solution and by comparisons with literature data.[26] The presence of pyridine in the external electrolyte, $CoP(py)/TiO_2$, did not change the order of this redox chemistry, but did influence the potentials at which they occurred.

The reduction of $Co^{II}P/TiO_2$ to $Co^{I}P/TiO_2$ was non-Nernstian under all conditions studied. The equilibrium potential at which the adjacent oxidation states were present in equal concentration was taken as the formal reduction potential. This was measured to be −720 mV and −850 mV vs NHE in the absence and presence of pyridine, respectively. The direction and magnitude of the pyridine-induced shift in the $E°(Co^{II/I})$ reduction potential was consistent with literature reports.[13] Spectroscopic titration data revealed significant spectral changes indicative of pyridine ligation to $Co^{II}P/TiO_2$, but no evidence for pyridine coordination when the Co center was in the formal oxidation state of Co^{I}. Therefore, the shift in reduction potentials can be attributed to the equilibrium shown in eq 5.

$$Co^{II}P/TiO_2 + py \overset{K_{eq}}{\rightleftharpoons} Co^{II}P(py)/TiO_2 \quad (5)$$

In the absence of pyridine, the acetonitrile solvent or a TiO_2 surface site likely serves as the fifth ligand for $Co^{II}P$, and the true equilibrium is therefore expected to be more complex than that shown in eq 5. If one assumes that inductive effects due to this nonpyridine ligation are small, the measured 130 mV shift in formal reduction potentials corresponds to $K_{eq} > 10^2\ M^{-1}$ for pyridine ligation to Co^{II}, a value in good agreement with previous studies in CH_2Cl_2 electrolytes.[13,27]

Anodic or cathodic potential steps greater than 59 mV were required to induce a factor of 10 change in the $[Co^{II}]:[Co^{I}]$ ratio when anchored to TiO_2, behavior that necessitated the inclusion of ideality factors to model this interfacial redox chemistry.[23] An ideality factor of 2.2, that is, about 130 mV/decade, was required to accurately model the data in the absence of pyridine and 1.6, 95 mV/decade, in the presence of pyridine. The molecular origins of nonideality at semiconductor interfaces remain unknown and speculative.[23,28] Nevertheless, this data demonstrates that ideality factors can be controlled by coordination of nonredox active molecules.

As the focus of this work was on electron transfer driven changes in the cobalt coordination number, it would have been convenient if pyridine had no influence on the TiO_2 redox chemistry; however, this was not found to be the case. Indeed pyridine, particularly *tert*-butyl pyridine, is a common additive in dye-sensitized solar cells that is known to increase open circuit photovoltages.[29−33] In LiI/I_2 acetonitrile electrolytes, the addition of *tert*-butyl pyridine to the electrolyte has been

Scheme 2. Summary of Interfacial Electron Transfer and Pyridine Coordination Kinetics

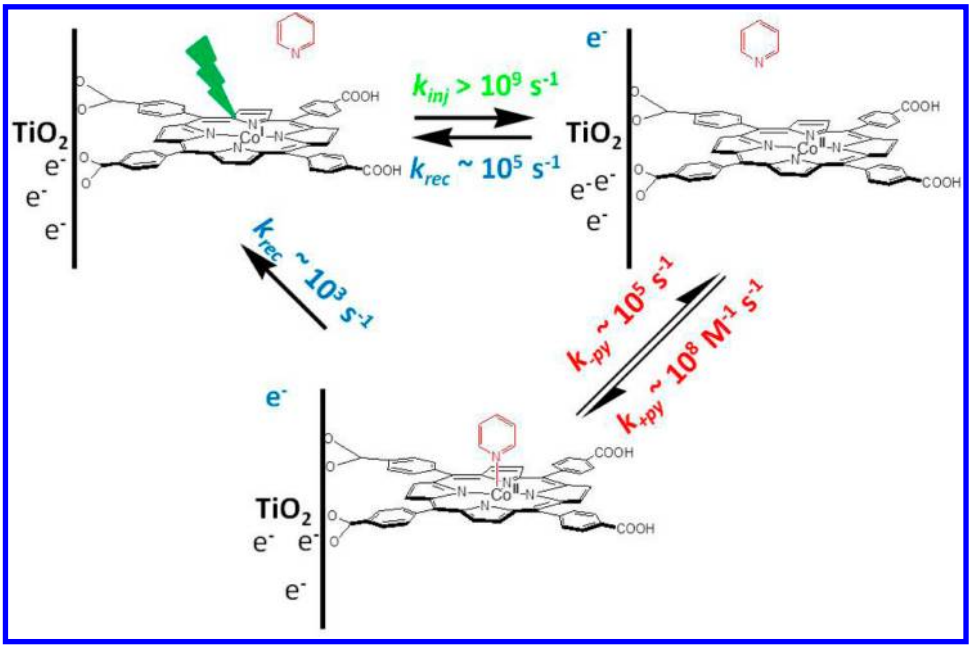

dx.doi.org/10.1021/ic301300h | *Inorg. Chem.* XXXX, XXX, XXX−XXX

shown to induce a negative potential shift in the TiO_2 density of states.[34,35] Under the conditions reported here with $TBAClO_4$/CH_3CN, the shift was in the same direction but smaller. Lewis base coordination to other semiconductor materials has also been shown to have a similar effect and, in general, is expected to lower the work function of solids.[36] Sigma donation from the pyridine lone pair would inductively be expected to increase the $Ti^{IV/III}$ reduction potential of acceptor states relative to a weaker Lewis base like CH_3CN. As the Ti centers in TiO_2 have a d^0 electronic configuration, π-backbonding is not expected to be significant in the fully reduced form although it may become more relevant after excited state injection and/or a forward bias generates Ti(III) states. An alternative explanation for the pyridine-induced shift is that pyridine acts as a Brønsted base that deprotonates surface titanol groups that gives rise to the Nernstian band edge shifts commonly reported for metal-oxide semiconductors with pH in aqueous solution.[37] Indeed, the TiO_2 thin films used herein were pretreated with aqueous base and studied in acetonitrile electrolytes without intentionally added "potential determining cations", such as Li^+ and H^+, so that $Co^{I}P$ could be generated with only a small concentration of $TiO_2(e^-)$s.[2]

Kinetics and Mechanisms. Pulsed-light excitation of $Co^{I}P/TiO_2$ resulted in spectral changes consistent with rapid excited state injection, $k_{inj} > 10^8$ s^{-1}, to yield $Co^{II}P/TiO_2(e^-)$. In the absence of pyridine, this was the only product observed spectroscopically. At high pyridine concentrations, a single product was again observed with spectroscopic features assigned to $Co^{II}P(py)/TiO_2(e^-)$ indicating that both excited state injection and pyridine coordination occurred within 10 ns, the response time of our apparatus. When pyridine was present at intermediate concentrations, a time dependent spectral change assigned to pyridine coordination to Co^{II} was observed that allowed the kinetics for Co^{II} coordination chemistry to be quantified. A second-order rate constant of $2 \pm 1 \times 10^8$ M^{-1} s^{-1} for pyridine coordination $Co^{II}P/TiO_2(e^-)$ was abstracted from kinetic data measured as a function of pyridine concentration and was consistent with that reported in solution, Scheme 2.[27,38]

The ~130 mV negative shift of $E°(Co^{II/I})$ that accompanied pyridine coordination to Co(II) decreased the driving force for $TiO_2(e^-)$ + $Co^{II}P(py)$ charge recombination by a corresponding value. We note that pyridine altered the reduction of TiO_2 itself, however this influence was small relative to the change in the metalloporphyrin reduction potential. Pyridine ligation decreased significantly the observed charge recombination rate constant. In making this comparison, care was taken to ensure that the $TiO_2(e^-)$ concentration was the same as it is now well established that recombination rates at sensitized TiO_2 interfaces are highly sensitive to the concentration of trapped electrons.[2,11] Indeed, charge recombination was on average 100 times faster when pyridine was absent over a factor of 3 change in $TiO_2(e^-)$ concentration, presumably because of the less favorable free energy change with electron transfer in the normal kinetic region.

Three mechanisms for $Co^{II}P(py)/TiO_2(e^-)$ charge recombination can be envisioned: (1) a concerted process wherein electron transfer and Co^{II}-py bond cleavage occur in one step; (2) electron transfer followed by Co^{I}-py bond breaking; and (3) Co^{II}-py bond cleavage followed by interfacial electron transfer. The second mechanism could have been unambiguously identified by the appearance of a Co^{I}-py intermediate. Despite many attempts, no evidence for such intermediates were garnered. Density functional calculations of cobalamin indicate that a 5-coordinate Co^{I} species is energetically unfavored.[39]

Establishment of the pyridine equilibrium and rate constant affords calculation of the rate constant for pyridine dissociation from $Co^{II}P(py)/TiO_2(e^-)$ to be $\sim 5 \times 10^5$ s^{-1}. Therefore, on average pyridine deligates from $Co^{II}P(py)/TiO_2$ every 1.4 μs and remains dissociated for 1 μs and 10 ns at 0.003 and 0.300 M pyridine concentrations, respectively. As a result, charge recombination that was observed to occur on a much slower millisecond time scale could indeed occur by a mechanism where pyridine dissociation occurred prior to back electron transfer. The derived rate law for such a mechanism is inversely correlated with the concentration of pyridine as was observed experimentally. Consequently, a stepwise mechanism where ligand dissociation occurs prior to electron transfer is most consistent with the data. We note that concerted electron transfer mechanisms have previously been invoked by Saveant and coworkers in cobalamin chemistry for dissociation of cobalt–carbon bonds, behavior that cannot be fully ruled for the Co-py bond breaking that accompanies the interfacial electron transfer data reported herein.[40]

CONCLUSIONS

The first instance of photoinduced interfacial electron transfer incurring a change in coordination number was observed and quantified. The coordination of pyridine to the $Co^{II}P/TiO_2(e^-)$ charge-separated state influenced both the kinetics and the thermodynamics for interfacial charge recombination. A factor of 100 decrease in the observed rate constant for charge recombination was quantified when pyridine was present. The charge recombination mechanism was not fully established, but the data were consistent with ligand dissociation followed by electron transfer.

ASSOCIATED CONTENT

Supporting Information

Absorption spectra of TiO_2 thin films with and without $TiO_2(e^-)$s. This material is available free of charge via the Internet at http://pubs.acs.org.

AUTHOR INFORMATION

Corresponding Author

*E-mail: meyer@jhu.edu.

Notes

The authors declare no competing financial interest.

ACKNOWLEDGMENTS

The National Science Foundation is gratefully acknowledged for research support.

REFERENCES

(1) Hagfeldt, A.; Grätzel, M. *Acc. Chem. Res.* **2000**, *33*, 269–277.
(2) Ardo, S.; Meyer, G. J. *Chem. Soc. Rev.* **2009**, *38*, 115–164.
(3) O'Regan, B.; Grätzel, M. *Nature* **1991**, *353*, 737–740.
(4) Youngblood, W. J.; Lee, S.-H. A.; Kobayashi, Y.; Hernandez-Pagan, E. A.; Hoertz, P. G.; Moore, T. A.; Moore, A. L.; Gust, D.; Mallouk, T. E. *J. Am. Chem. Soc.* **2009**, *131*, 926–927.
(5) Brimblecombe, R.; Koo, A.; Dismukes, G. C.; Swiegers, G. F.; Spiccia, L. *J. Am. Chem. Soc.* **2010**, *132*, 2892–2894.
(6) Gleria, M.; Memming, R. *Z. Phys. Chem.* **1975**, *98*, 303–316.
(7) Anderson, S.; Constable, E. C.; Dare-Edwards, M. P.; Goodenough, J. B.; Hamnett, A.; Seddon, K. R.; Wright, R. D. *Nature* **1979**, *280*, 571–573.

(8) Gilbert, J. A.; Eggleston, D. S.; Murphy, W. R., Jr.; Geselowitz, D. A.; Gersten, S. W.; Hodgson, D. J.; Meyer, T. J. *J. Am. Chem. Soc.* **1985**, *107*, 3855−3864.
(9) Hurst, J. K.; Cape, J. L.; Clark, A. E.; Das, S.; Qin, C. *Inorg. Chem.* **2008**, *47*, 1753−1764.
(10) Wasylenko, D. J.; Ganesamoorthy, C.; Henderson, M. A.; Koivisto, B. D.; Osthoff, H. D.; Berlinguette, C. P. *J. Am. Chem. Soc.* **2010**, *132*, 16094−16106.
(11) Achey, D.; Ardo, S.; Xia, H.-L.; Siegler, M. A.; Meyer, G. J. *J. Phys. Chem Lett.* **2011**, *2*, 305−308.
(12) Lexa, D.; Saveant, J. M. *Acc. Chem. Res.* **1983**, *16*, 235−243.
(13) Kadish, K.; Bottomley, L. A.; Beroiz, D. *Inorg. Chem.* **1978**, *17*, 1124−1129.
(14) Blaskie, M. W.; McMillin, D. R. *Inorg. Chem.* **1980**, *19*, 3519−3522.
(15) Chen, L. X.; Jennings, G.; Liu, T.; Gosztola, D. J.; Hessler, J. P.; Scaltrito, D. V.; Meyer, G. J. *J. Am. Chem. Soc.* **2002**, *124*, 10861−10867.
(16) Ruthkosky, M.; Kelly, C. A.; Zaros, M. C.; Meyer, G. J. *J. Am. Chem. Soc.* **1997**, *119*, 12004−12005.
(17) Scaltrito, D. V.; Kelly, C. A.; Ruthkosky, M.; Zaros, M. C.; Meyer, G. J. *Inorg. Chem.* **2000**, *39*, 3765−3770.
(18) Hino, J. K.; Ciana, L. D.; Dressick, W. J.; Sullivan, B. P. *Inorg. Chem.* **1992**, *31*, 1072−1080.
(19) Hasselmann, G. M.; Meyer, G. J. *J. Phys. Chem B* **1999**, *103*, 7671−7675.
(20) Heimer, T. A.; D'Arcangelis, S. T.; Farzad, F.; Stipkala, J. M.; Meyer, G. J. *Inorg. Chem.* **1996**, *35*, 5319−5324.
(21) Argazzi, R.; Bignozzi, C. A.; Heimer, T. A.; Castellano, F. N.; Meyer, G. J. *Inorg. Chem.* **1994**, *33*, 5741−5749.
(22) Bard, A. J.; Faulkner, L. R. *Electrochemical Methods: Fundamentals and Applications*, 2nd ed.; Wiley: New York, 2001.
(23) Ardo, S.; Achey, D.; Morris, A. J.; Abrahamsson, M.; Meyer, G. J. *J. Am. Chem. Soc.* **2011**, *133*, 16572−16580.
(24) Williams, G.; Watts, D. C. *Trans. Faraday Soc.* **1970**, *66*, 80−85.
(25) Lindsey, C. P.; Patterson, G. D. *J. Chem. Phys.* **1980**, *73*, 3348−3357.
(26) D'Souza, F.; Villard, A.; Van Caemelbecke, E.; Franzen, M.; Boschi, T.; Tagliatesta, P.; Kadish, K. M. *Inorg. Chem.* **1993**, *32*, 4042−4048.
(27) Tetreau, C.; Lavalette, D.; Momenteau, M. *J. Am. Chem. Soc.* **1983**, *105*, 1506−1509.
(28) Zaban, A.; Ferrere, S.; Gregg, B. A. *J. Phys. Chem. B* **1998**, *102*, 452−460.
(29) Nazeeruddin, M. K.; Kay, A.; Rodicio, I.; Humphry-Baker, R.; Mueller, E.; Liska, P.; Vlachopoulos, N.; Grätzel, M. *J. Am. Chem. Soc.* **1993**, *115*, 6382−6390.
(30) Gothelid, M.; Yu, S.; Ahmadi, S.; Sun, C.; Zuleta, M. *Int. J. Photoenergy* **2011**, 2011.
(31) Yu, S.; Ahmadi, S.; Sun, C.; Palmgren, P.; Hennies, F.; Zuleta, M.; Gothelid, M. *J. Phys. Chem. C* **2010**, *114*, 2315−2320.
(32) Shi, C.; Dai, S.; Wang, K.; Pan, X.; Kong, F.; Hu, L. *Vib. Spectrosc.* **2005**, *39*, 99−105.
(33) Xiong, Y.; Weiwei, T.; Jingbo, Z.; Yuan, L.; Xurui, X.; Xiaowen, Z.; Xueping, L.; Sankapal, B. R. *J. App. Electrochem.* **2009**, *39*, 147−154.
(34) Hara, K.; Dan-oh, Y.; Kasada, C.; Ohga, Y.; Shinpo, A.; Suga, S.; Sayama, K.; Arakawa, H. *Langmuir* **2004**, *20*, 4205−4210.
(35) Boschloo, G.; Haggman, L.; Hagfeldt, A. *J. Phys. Chem. B* **2006**, *110*, 13144−13150.
(36) Stair, P. C. *J. Am. Chem. Soc.* **1982**, *104*, 4044−4052.
(37) Finklea, H. O. *Semiconductor Electrodes*; Elsevier: New York, 1988.
(38) Gouterman, M.; Tait, C. D.; Holten, D. *J. Am. Chem. Soc.* **1984**, *106*, 6653−6659.
(39) Brunold, T. C.; Liptak, M. D. *J. Am. Chem. Soc.* **2008**, *128*, 9144−9156.
(40) Costentin, C.; Robert, M.; Saveant, J.-M. *J. Am. Chem. Soc.* **2005**, *127*, 12154−12155.